

Similarity solutions for breakup of jets of power law fluids

Michael and Yuriko Renardy
Department of Mathematics
Virginia Polytechnic Institute and State University
Blacksburg, Virginia 24061-0123, USA

January 12, 2004

Abstract

We compute similarity solutions for the breakup of a jet of a power law liquid surrounded by a vacuum. As is known from the Newtonian case, such similarity solutions are fundamentally different depending on whether creeping flow or flow with inertia is considered. We shall investigate both cases. For flow with inertia, we start with Eggers' solution for the Newtonian case, and we continue it to other values of the power law exponent. The jet profile corresponding to Eggers' solution is highly asymmetric. We find that the degree of asymmetry decreases as we deviate from the Newtonian case in either direction. For small as well as for large values of the power law exponent, we find new branches of symmetric solutions. These branches establish a connection between the similarity solutions with and without inertia.

Keywords: Jet breakup, similarity solution, power law fluid,

1 Introduction

Recent work has shown that the pinching of liquid threads under the influence of surface tension can be described by similarity solutions of a simplified one-dimensional slender body model. For Newtonian fluids, Papageorgiou [9] analyzed the case of Stokes flow. The work of Eggers [6, 7] has shown,

however, that the inclusion of inertia significantly changes the picture. No matter how viscous the liquid is, inertia eventually enters into the dominant balance as breakup is approached, and a solution whose qualitative features are very different from the Stokes flow solution describes the final stage of pinching. The transition from the ‘Papageorgiou’ to ‘Eggers’ asymptotics is verified experimentally in [13]. Lister and Stone [8] have shown that the situation is more complicated still when the viscosity of an outer fluid is significant. In that case, the ultimate breakup is governed by Stokes flow with negligible inertia.

In the following, we focus on the generalized Newtonian fluid with a power law viscosity. For the case without inertia, the existence of similarity solutions is proved in [10]. Computations of similarity solutions are reported in [4], where the range of the power law exponent, defined in the next section, is restricted to $1/2 \leq a \leq 1$. In Section 3, we extend the computation to cover all values of a .

Doshi *et al.* [3] undertake a full numerical simulation of the one-dimensional equations for jets of power law fluids. Both the creeping flow case and the case including inertia are considered. Their results indicate that the long-time behavior of solutions to the initial value problem is consistent with self-similar breakup. In this paper, therefore, we solve the ODE system governing self-similar solutions directly. Section 4 addresses the computation of self-similar solutions for the case with inertia. We find that the Eggers solution continues on a branch through the interval $0.3 \leq a \leq 1.97$. Outside this interval, on the other hand, the assumption of neglecting inertia becomes consistent, and the inertialess solution becomes valid even when inertia is present. We may therefore expect a transition from the inertialess to the inertial case. Such a transition, however, cannot be a conventional bifurcation, since the scaling of variables to arrive at the two types of similarity solution is different. We find that the link between the inertial and inertialess cases is provided by new branches of symmetric solutions of the inertial case. These branches end in singular limits at which the inertial solutions develop a singularity. This singularity, however, can be removed by rescaling, and the solution then becomes equivalent to the solution without inertia.

We note that the question of the “right” power law exponent for elongational flows of polymeric liquids is much less straightforward than for shear flows. While most polymeric liquids shear thin, they can be thickening or thinning in elongation. Molecular models for solutions, which are based on considering individual polymer molecules, predict elongation thickening,

until a limit of the elongational viscosity is reached when molecules reach their maximum extension. We refer to Entov and Hinch [5] for a discussion of these regimes and comparison with experiments in the context of the FENE-P model. Theories of entangled polymers, on the other hand, predict elongation thinning. The behavior can change to elongation thickening at higher deformation rates, when deformation of individual chains becomes more important than the dynamics of entanglement. On the other hand, some experiments, see e.g. [1] show elongation thinning persisting at high elongation rates, at least over the range of observations (they find a power law exponent of $a \sim 0.5$). Suspensions can also be elongation thinning. Due to this variety of possible behaviors, it is worthwhile to investigate all values of the power law exponent rather than just the elongation thinning range as in [4].

As a caution, we note that polymeric liquids are not really power law fluids at all. It is established in [11] that similarity solutions for breakup can behave quite differently for different models, even if the elongational viscosity as a function of elongation rate is similar. Characteristics of the breakup of jets can thus serve as a criterion to distinguish between classes of models. The analysis in [11] covers only inertialess solutions. The study of similarity solutions with inertia is significantly more difficult and is currently in its infancy. Renardy and Losh [12] considered the Giesekus model and found little qualitative difference with the Newtonian case. The present analysis of power law fluids shows more interesting behavior. How the inclusion of memory and the various models allowing for such inclusion will affect the results remains to be investigated.

2 Governing equations

The Lagrangian description is adopted for the formulation of the governing equations. This is consistent with earlier works [10]-[12]. We consider a free jet, with an undisturbed uniform reference configuration. Let δ denote the radius of the unperturbed uniform jet. All variables are regarded as functions of the position X of a particle in the undisturbed uniform jet and time t . As the jet deforms, the position of such a particle in space is given by a function $x(X, t)$. Let s denote the amount of stretch:

$$s = \frac{\partial x}{\partial X}. \tag{1}$$

A slender body approximation is applied: s , the axial velocity u , the axial and radial stress components T_{11} and T_{rr} , and the hydrostatic pressure p are assumed to be constant in a cross-section of the jet. As a result of incompressibility, the radius r of a cross-section of the jet after stretching is

$$r = \frac{\delta}{\sqrt{s}}. \quad (2)$$

The force in the cross-section has components from the stress ($\pi r^2(T_{11} - p)$) and surface tension ($2\pi r\sigma$), where σ denotes the surface tension coefficient. With ρ denoting the density, Newton's law leads to

$$\pi\delta^2\rho u_t = \frac{\partial}{\partial X}[\pi r^2(T_{11} - p) + 2\pi r\sigma]. \quad (3)$$

On the lateral surface of the jet, the normal stress is balanced by surface tension:

$$T_{rr} - p = -\frac{\sigma}{r}. \quad (4)$$

(2) and (4) are used to eliminate r and the pressure p in (3):

$$\rho u_t = \frac{\partial}{\partial X}\left[\frac{T_{11} - T_{rr}}{s} + \frac{\sigma}{\delta\sqrt{s}}\right]. \quad (5)$$

Moreover, the equality of mixed partial derivatives implies that

$$s_t = u_X. \quad (6)$$

The stress is assumed to be described by a power law viscosity:

$$T_{11} = 2\eta\frac{s_t}{s}\left|\frac{s_t}{s}\right|^{a-1}, \quad T_{rr} = -\eta\frac{s_t}{s}\left|\frac{s_t}{s}\right|^{a-1}. \quad (7)$$

3 The inertialess case

If inertia is neglected, we may set $\rho = 0$ in (5). Integration of the equation with respect to X then yields

$$3\eta\frac{s_t}{s}\left|\frac{s_t}{s}\right|^{a-1} + \frac{\sigma}{\delta}s^{1/2} = \lambda(t)s, \quad (8)$$

where $\lambda(t)$ is an undetermined function of t , which is independent of X . We can set $t = (3\eta\delta/\sigma)^{1/a}\tilde{t}$ and $\lambda = \sigma\tilde{\lambda}/\delta$ to eliminate the constants 3η and σ/δ from the equation; this leads to the dimensionless form

$$\frac{s_t}{s} \left| \frac{s_t}{s} \right|^{a-1} + s^{1/2} = \lambda(t)s, \quad (9)$$

We note that the equations have a scaling invariance under the transformation $X \rightarrow qX$, $u \rightarrow qu$. This scaling invariance reflects the fact that the physical constants can be combined to form a velocity scale, but not a length or time scale.

We seek self-similar solutions of the form

$$s(X, t) = (-t)^{-\alpha} \phi\left(\frac{X}{(-t)^\beta}\right), \quad \lambda(t) = k(-t)^\gamma. \quad (10)$$

This, together with

$$\xi = \frac{X}{(-t)^\beta}, \quad (11)$$

transforms (8) to

$$\begin{aligned} (-t)^{-a}(\alpha\phi + \beta\xi\phi')|\alpha\phi + \beta\xi\phi'|^{a-1} + (-t)^{-\alpha/2}\phi^{a+1/2} \\ - k(-t)^{\gamma-\alpha}\phi^{a+1} = 0. \end{aligned} \quad (12)$$

By matching terms in this equation, we find $\alpha = 2a$, $\gamma = a$, and

$$(\alpha\phi + \beta\xi\phi')|\alpha\phi + \beta\xi\phi'|^{a-1} + \phi^{a+1/2} - k\phi^{a+1} = 0. \quad (13)$$

A physical condition for a similarity solution is that there should not be large velocities outside the self-similar region. According to (6), this translates into the requirement that

$$\int_{-\infty}^{\infty} s_t dX = 0, \quad (14)$$

and hence

$$\int_{-\infty}^{\infty} 2a\phi(\xi) + \beta\xi\phi'(\xi) d\xi = 0. \quad (15)$$

At fixed t , s has a maximum at the breakup point $X = 0$. Hence $\phi(\xi)$ has a maximum at $\xi = 0$. If ϕ is smooth at $\xi = 0$, then generically, we have

$$\phi(\xi) = y_0 - y_2\xi^2 + \dots, \quad (16)$$

which determines β and k in terms of y_0 [10]:

$$k = \frac{(2a)^a}{y_0} + \frac{1}{\sqrt{y_0}}, \quad \beta = 1 + 2^{-1-a} y_0^{1/2} a^{-a}. \quad (17)$$

The expression given for β in [10] contains an error.

Bounds on β are obtained as follows. The first term in (15) is integrated by parts, noting that ϕ is a symmetric function of ξ and $\phi \rightarrow 0$ as $\xi \rightarrow \pm\infty$:

$$\int_{-\infty}^{\infty} 2a\phi(\xi) d\xi = \lim_{M \rightarrow \infty} \left(4aM\phi(M) - 2a \int_{-M}^M \xi\phi'(\xi) d\xi \right). \quad (18)$$

(15) becomes

$$0 = (\beta - 2a) \int_{-\infty}^{\infty} \xi\phi'(\xi) d\xi + 4a \lim_{M \rightarrow \infty} M\phi(M). \quad (19)$$

Both terms on the right hand side are positive unless $\beta > 2a$. Moreover, it is shown in [10] that $\beta < 2a + 1$. We conclude that $2a < \beta < 2a + 1$.

For a fixed a , the numerical solution of (13) and (15) proceeds as follows. Two values of y_0 are found, one that makes the integral in (15) positive and one that makes it negative. For any positive y_0 , we can numerically solve (13), and the integral term in (15) is finite as long as $\beta < 2a + 1$. If y_0 is sufficiently small, the integral term is positive, while it becomes negative when β is close to $2a + 1$ [10]. To the pair of y_0 values, a bisection method is applied, to find the value of y_0 for which the integral is equal to zero. Finally, (17) gives β as a function of y_0 and a .

Figure 1 shows that β is close to $2a + 1$ for small a , and close to $2a$ for large a . We note that, heuristically, elongation thinning would be expected to weaken the jet as breakup is approached, enhancing the nonuniformity of the jet thickness. Indeed, the radius of the jet away from the breakup point as a function of spatial position behaves as $r \sim x^{a/(\beta-2a)}$ as discussed in detail in the following section. For small a , this is approximately $r \sim x^a$, indicating a cusped profile. Indeed, the slender body approximation, which neglects axial relative to azimuthal curvature, is inconsistent if $a/(\beta - 2a) < 1$. i.e. $\beta > 3a$. If a is large, on the other hand, then $a/(\beta - 2a)$ becomes very large, since $\beta - 2a \rightarrow 0$ as shown in Figure 1. Hence jet profiles become very flat.

The role of inertia is harder to assess at the heuristic level. Naively, one might expect that elongation thinning makes viscosity less important at high elongation rates, and so inertia should become more important. Such an

argument, however, assumes fixed kinematics, and the kinematics itself depends on the value of the power law exponent a . It turns out that, as breakup is approached, the extension rate behaves like $-1/t$ and the viscous stress therefore behaves like $(-t)^{-a}$. The spatial length of the self-similar region behaves like $(-t)^{\beta-2a}$, and so the maximal velocity behaves like $(-t)^{\beta-2a-1}$ and the Reynolds stress is proportional to $(-t)^{2\beta-4a-2}$. By comparing Reynolds stresses and viscous stresses, we find that inertia needs to be considered close to breakup if $\beta < 3a/2 + 1$.

The lines $\beta = 3a$ and $\beta = 3a/2 + 1$ are drawn dashed in Figure 1; the bold dots denote intersections and show that inertia can be neglected only if a is either less than about 0.26 or larger than approximately 1.95; *i.e.*, for fluids that are either strongly shear thinning or strongly shear thickening. Axial curvature is important if a is less than approximately 0.54.

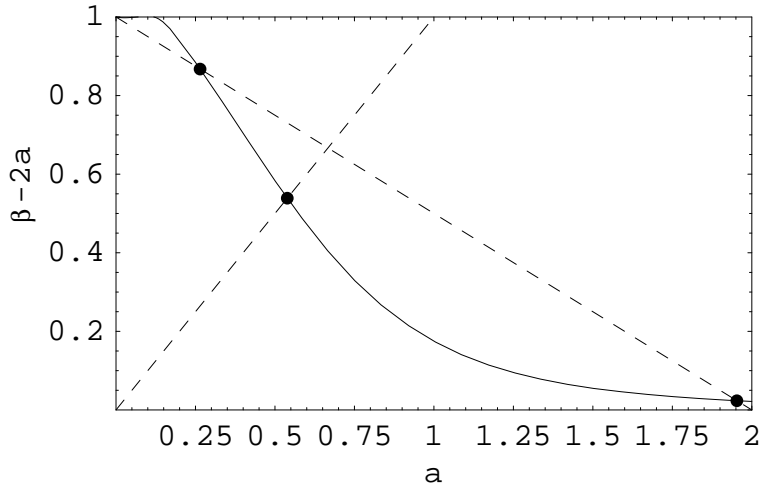


Figure 1: Case without inertia. Similarity exponent $\beta - 2a$ as a function of the power law exponent a .

In this paper, we shall ignore the effect of axial curvature. As we saw, this assumption is incorrect for $a < 0.54$, and we shall find it to be similarly incorrect if $a < 2/3$ for solutions with inertia. The physical validity of our solutions is restricted by this. Our analysis cannot describe the behavior all the way to breakup, rather it is limited to describing the evolution of long waves which are “long” because of an appropriate choice of initial data rather than because of the intrinsic dynamics of the jet.

The main purpose of this paper is to investigate the transition from inertial to inertialess behavior. For the Newtonian case ($a = 1$), the two solutions are known to be very different. On the other hand, for small and large values of a , inertialess solutions are valid even if inertia is included in the analysis, and one may expect a transition from one behavior to the other. On the other hand, the scalings leading to a similarity solution differ in the inertial and inertialess case, so we cannot simply have one type of solution bifurcating from the other. As we shall see below, there are branches of symmetric inertial solutions for both small and large a which connect to the inertialess solution in a singular limit. Over a small interval, these branches of symmetric solutions coexist with the asymmetric branch which is obtained by continuation of Eggers' Newtonian solution.

4 The case with inertia

We can eliminate the constants ρ , 3η and σ/δ from the equations by rescaling. Specifically, from the three physical constants, ρ , η and σ , we can form a timescale $\tau = [27\eta^3/(\rho\sigma^2)]^{1/(3a-2)}$ and a lengthscale $L = (\tau^2\sigma/\rho)^{1/3}$. Since δ has no intrinsic physical meaning, we can set it equal to L and use these length and time scales for nondimensionalization. In dimensionless form, (5) becomes

$$\begin{aligned} u_t &= \frac{\partial}{\partial X} \left(\frac{s_t}{s^2} \left| \frac{s_t}{s} \right|^{a-1} + \frac{1}{\sqrt{s}} \right), \\ s_t &= u_X. \end{aligned} \quad (20)$$

We seek self-similar solutions of the form

$$\begin{aligned} s(X, t) &= (-t)^{-\alpha} \phi \left(\frac{X}{(-t)^\beta} \right), \\ u(X, t) &= (-t)^{-\gamma} \psi \left(\frac{X}{(-t)^\beta} \right). \end{aligned} \quad (21)$$

Substitution into (20) and equating coefficients of like powers of t yields $\alpha + 1 = \beta + \gamma$, $\alpha = 2a$, and $\gamma + 1 = -(\alpha/2) + \beta$. This results in

$$\alpha = 2a, \quad \beta = \frac{3a}{2} + 1, \quad \gamma = \frac{a}{2}, \quad (22)$$

$$\begin{aligned} \gamma\psi + \beta\xi\psi' &= \frac{d}{d\xi} \left(\frac{\alpha\phi + \beta\xi\phi'}{\phi^2} \left| \alpha + \beta\xi\frac{\phi'}{\phi} \right|^{a-1} + \phi^{-1/2} \right), \\ \alpha\phi + \beta\xi\phi' &= \psi'. \end{aligned} \quad (23)$$

When $\beta < \alpha$ ($a > 2$), the reasoning given in [11] shows that the self-similar region expands rather than shrinks in space as breakup is approached. Such a solution cannot describe breakup in a problem which has boundary conditions imposed at a finite length. Indeed, we saw in the previous section that the assumption of no inertia is consistent for $a > 2$, and we should expect to observe that solution.

Near $\xi = 0$, we impose the condition that the solutions are analytic, and have the series expansions

$$\begin{aligned}\phi(\xi) &= s_0 + s_1\xi + s_2\xi^2 + s_3\xi^3 + \dots, \\ \psi(\xi) &= u_0 + u_1\xi + u_2\xi^2 + u_3\xi^3 + \dots\end{aligned}\tag{24}$$

Substitution in (23) shows that the coefficients s_n and u_n can be determined in terms of s_0 and u_0 , except at singular values of s_0 given by

$$\sigma_n = (2a)^{2a} \left(n - 2 + \frac{3n}{2}a\right)^2.\tag{25}$$

At $s_0 = \sigma_n$, $n = 1, 2, \dots$, the coefficient s_n becomes infinite and logarithmic terms must be included in the expansion (24).

As $\xi \rightarrow \infty$, ϕ and ψ decay to zero. The leading terms near infinity are

$$\begin{aligned}\phi(\xi) &= p_0\xi^{-\alpha/\beta} + p_1\xi^{-(\alpha+1)/\beta} + \dots, \\ \psi(\xi) &= q_0\xi^{-\gamma/\beta} + q_1\xi^{-(\gamma+1)/\beta} + \dots,\end{aligned}\tag{26}$$

because these make the left hand sides in (23) equal to zero and produce terms of lower order on the right hand sides. Substitution in (23) determines p_n and q_n in terms of p_0 and q_0 which are arbitrary. The Eulerian spatial position x is proportional to the integral of the stretch ϕ ; that is,

$$x \sim \xi^{1-\alpha/\beta}.\tag{27}$$

The radius of the jet is proportional to $\phi^{-1/2}$; *i.e.*,

$$r \sim \xi^{\alpha/(2\beta)}, \quad \xi \rightarrow \infty.\tag{28}$$

The values for α and β in (22) give the jet profile

$$r \sim x^{2a/(2-a)}, \quad \xi \rightarrow \infty.\tag{29}$$

When $2a/(2-a) < 1$ ($a < 2/3$), the jet becomes more cusped as breakup is approached ($t \rightarrow 0$, $\xi \rightarrow \pm\infty$). As noted in [3], this case is inconsistent

with the assumption underlying the model that the axial curvature can be neglected relative to the azimuthal curvature. The velocity ψ in terms of x behaves like $x^{-a/(2-a)}$ for $x \rightarrow \infty$.

The differential system (23) is of third order, so that a general solution has three arbitrary constants. On the other hand, according to the expansions discussed above, there is only a two-parameter family of solutions which are analytic at zero, and only a two-parameter family of solutions which have correct behavior at infinity. Each family describes a surface in a three-parameter space, and solutions that satisfy both are found along their intersection which is a line. This means that only a one-parameter family of solutions is expected. In terms of the coefficients in (24), this one-parameter family is characterized by a curve, say $h(s_0, u_0) = 0$. Analyticity at $\xi = 0$ and decay at $\xi \rightarrow -\infty$ determines another one-parameter family of solutions. In this case, reversing the sign of ψ and ξ leaves (23) invariant, giving the one-parameter family of solutions $h(s_0, -u_0) = 0$. A similarity solution valid for all ξ is found where the curves $h(s_0, u_0) = 0$ and $h(s_0, -u_0) = 0$ intersect.

In order to solve (23) numerically, it is transformed to a first-order system:

$$\begin{aligned} \gamma\psi + \beta\xi\psi' &= \frac{d}{d\xi}\left(\frac{w}{\phi} + \phi^{-1/2}\right), \\ \alpha\phi + \beta\xi\phi' &= \psi', \\ \alpha + \beta\xi\frac{\phi'}{\phi} &= |w|^{1/a} \text{sign}(w), \end{aligned} \tag{30}$$

where

$$w = \left(\alpha + \beta\xi\frac{\phi'}{\phi}\right) \left|\alpha + \beta\xi\frac{\phi'}{\phi}\right|^{a-1}. \tag{31}$$

We use the expansion (24) to generate initial conditions at $\xi = \delta$ where δ is small. Terms up to order δ^4 are taken into account (we have carefully checked the relative magnitude of successive terms in the expansion to ensure this is sufficient).

As in [12], we use a shooting method. Since we have to integrate (30) over many orders of magnitudes in ξ , we change variables to

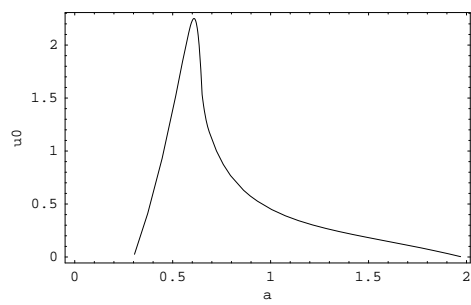
$$\zeta = \ln \xi. \tag{32}$$

The transformed version of (30) is solved numerically with the Mathematica command `NDSolve`. We fix a value of u_0 and try to adjust s_0 to obtain the correct behavior at infinity. Solutions which fail to have the correct

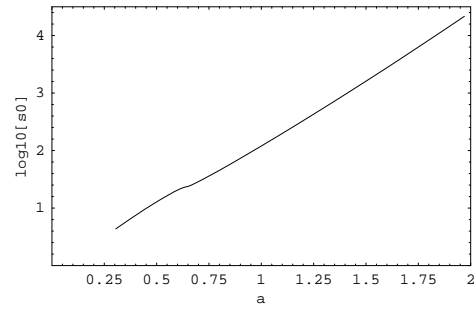
asymptotics at infinity either have $\psi(\xi) \rightarrow -\infty$ logarithmically or $\psi(\xi) \rightarrow +\infty$ at a finite ξ (see the examples shown in [12]). As a criterion for the shooting method, we therefore pick a sufficiently large value ξ_m of ξ and look for solutions which satisfy $\psi(\xi_m) = 0$.

The values of a in the results that follow are in the range between 0.18 and 2. Our choices for δ and ξ_m depend on a . At the upper end of the range, it is important to choose δ small enough and ξ_m large enough. We use $\delta = 10^{-6}$ and $\xi_m = 10^{15}$. For small values of a , on the other hand, $\xi_m = 10^6$ is more than sufficient, and if δ is chosen too small, numerical inaccuracy is encountered. We use $\delta = 10^{-4}$. In NDSolve, the step size for the variable ζ (32) is capped at either 0.0001 or 0.00005.

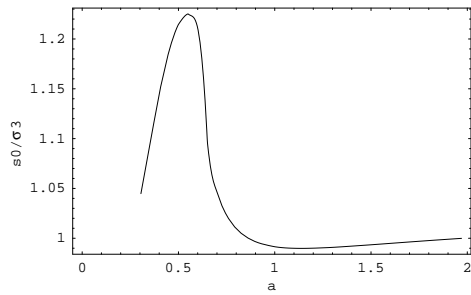
The Newtonian solution found by Eggers [2, 6, 7] corresponds to $a = 1$, $s_0 = 119.97$, $u_0 = 0.453$. The branch of solutions emanating from this is followed as a varies: we refer to this as the ‘Eggers’ branch. Figure 2 shows the variation of u_0 and $\log_{10}(s_0)$ with a . The value of s_0 on this branch is close to the third singular value σ_3 in (25), as noted in [2] for the Newtonian case. Note that σ_3 increases in orders of magnitude as a increases from 0 to 2. Part c of Figure 2 also shows the ratio s_0/σ_3 , and illustrates the relatively high disparity at a around 0.5. The Eggers branch extends from $a \approx 0.3$ at one end to $a \approx 1.97$ at the other. What happens to this branch at the two endpoints is different, although $u_0 \rightarrow 0$ at both. At $a \approx 0.3$, the Eggers branch bifurcates from a branch of symmetric solutions. At $a \approx 1.97$, the Eggers branch approaches the third singular value and the jet remains asymmetric, as we shall see from the jet profiles shown in the next section.



(a) u_0



(b) $\log_{10}(s_0)$



(c) s_0/σ_3

Figure 2: Velocity u_0 , logarithm of stretch s_0 and ratio of s_0 to the singular value σ_3 on the Eggers branch, as functions of the power law exponent a .

In principle, there is no reason why there should not be spatially symmetric solutions satisfying $s_{2n+1} = 0$, $n = 1, 2, \dots$. In the Newtonian case, none were ever found, although people have searched for them. Our calculations show that branches of symmetric solutions are found near both $a = 0.3$ (Figure 4) and $a = 1.97$ (Figure 3). These symmetric solution branches will be seen to be the ones which make the connection from breakup with inertia to breakup without inertia. At the lower end, the Eggers branch joins onto the symmetric solution at a bifurcation point. Each symmetric branch exists over a fairly narrow interval of a , in which s_0 begins at the second singular value and terminates at the fourth. These singular values are plotted in the figures by dashed lines. At these end-points, the solution becomes identical to the inertialess solution described in Section 3, modulo a rescaling of the similarity variable ξ (this rescaling, of course, becomes singular in the limit $\rho \rightarrow 0$). The case $s_0 = \sigma_2$ corresponds to solutions (24) that have quadratic behavior near the breakup point $\xi = 0$. The values of a at which the symmetric branches join onto the second singular value coincide with the two points of intersection of the inertialess curve $\beta(a)$ in Figure 1 with the inertial solution (22) $\beta = 3a/2 + 1$ (dashed in Figure 1). When s_0 is at the fourth singular value, the solution corresponds to a second family of inertialess solutions that is not discussed in Section 3, for which the series expansion around $\xi = 0$ (16) is replaced by $\phi(\xi) = y_0 - y_4\xi^4 + \dots$. Our numerical results gave no indication of a solution branch on the other side of the singular limit points.

The stability of solutions remains an open problem. The question is of particular interest on those intervals of the parameter a where several solutions coexist. In the Newtonian case, the Eggers solution was found numerically to be the profile towards which a general solution evolves. An analysis in [2] provides reasons why this solution is the least unstable of an infinite family of similarity solutions. Heuristically, we may expect the inertialess solution to be stable where neglecting inertia is consistent, i.e. for $a > 1.95$ and $a < 0.26$; we may then expect the stability to be transferred to the symmetric branch bifurcating at these points and ultimately to the Eggers branch. This expectation needs to be verified by simulations of initial value problems.

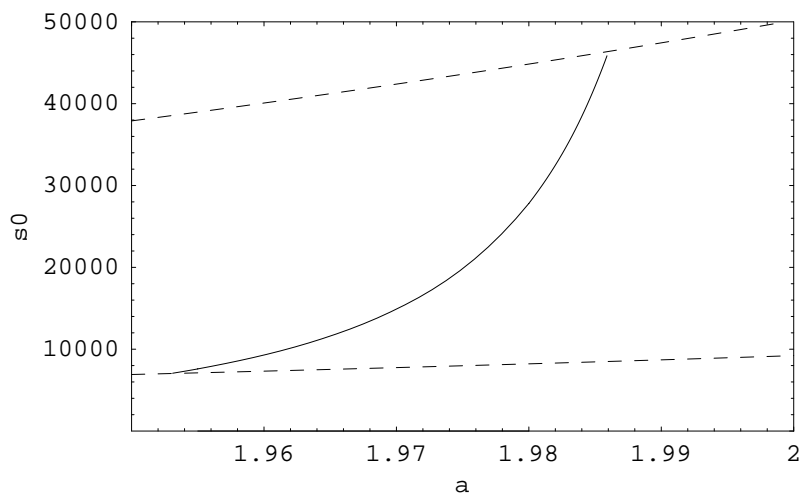


Figure 3: Branch of symmetric solutions (solid) for a close to 2. Included in this plot are the singular values (dashed) σ_2 and σ_4 . The solution reaches $s_0 = \sigma_2$ at the same value of a as the intersection of β with the curve $3a/2+1$ in Figure 1.

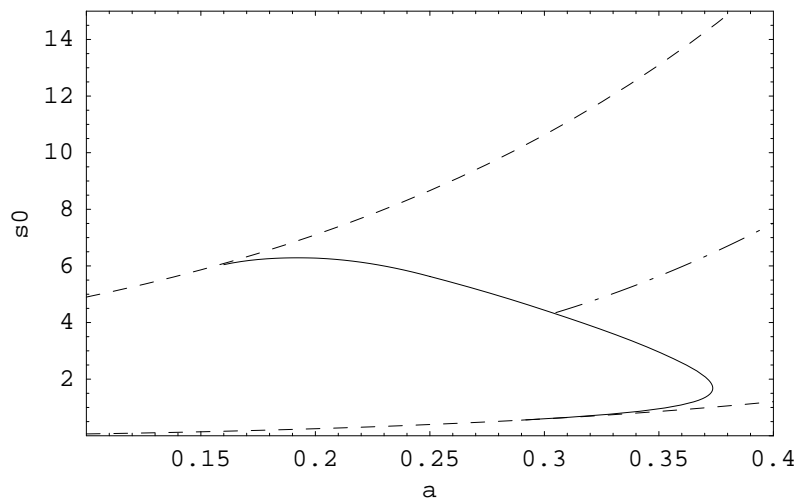
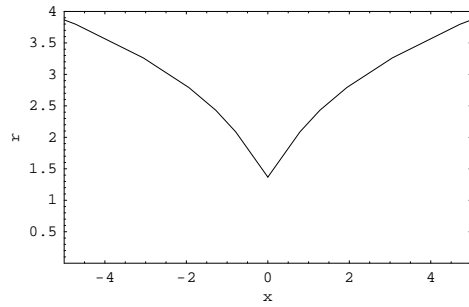


Figure 4: Branch of symmetric solutions for a close to 0.3 (solid). The lower dashed curve is σ_2 vs a , and the upper dashed curve is σ_4 . The solution intersects σ_2 at the same value of a where β intersects the line $3a/2 + 1$ in Figure 1. The Eggers branch, indicated by the dash-dotted line, bifurcates from this solution.

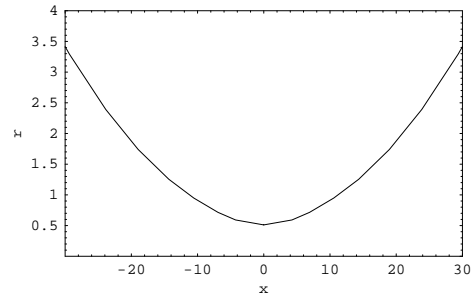
5 Jet profiles

The profile of the jet is presented in physical space. The jet radius $r = 1/\sqrt{\phi(\xi)}$ is plotted against the Eulerian spatial position $x = \int_0^\xi \phi(\eta) d\eta$. For large ξ , (28) gives $r \sim x^{\alpha/(2(\beta-\alpha))}$, where $\alpha = 2a$ and $\beta = 3a/2 + 1$ for the case with inertia, and β is given in Figure 1 for the case without inertia. The shape for large x is convex if $\beta < 3a$ and concave if $\beta > 3a$.

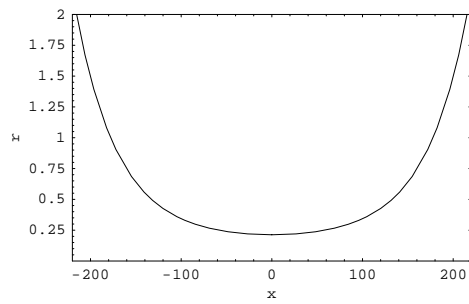
In the inertialess case, $\beta - \alpha$ tends to zero as $a \rightarrow \infty$ and becomes quite small near $a = 2$, while in the case with inertia $\beta - \alpha$ would reach 0 at $a = 2$ (we have not found any solution in this case which actually extends to $a = 2$). For a close to 2, therefore, r behaves like a large power of x , leading to a jet profile which is very flat at the center and then rises very steeply. Figure 5 shows jet profiles for the inertialess case and illustrate these trends.



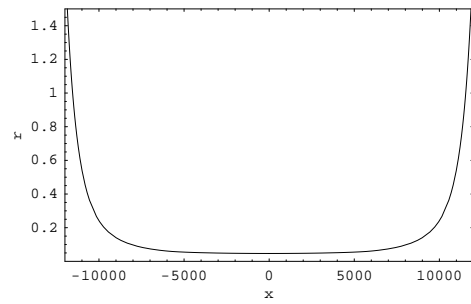
(a) $a = 0.3$



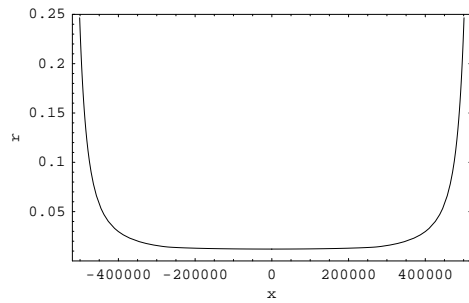
(b) $a = 0.7$



(c) $a = 1.0$



(d) $a = 1.5$

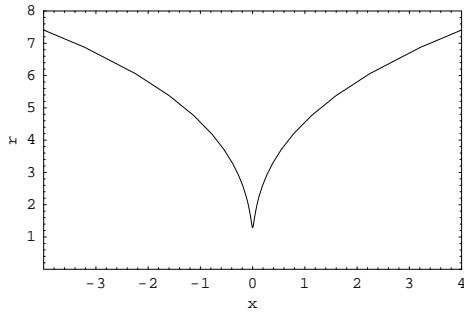


(e) $a = 1.98$

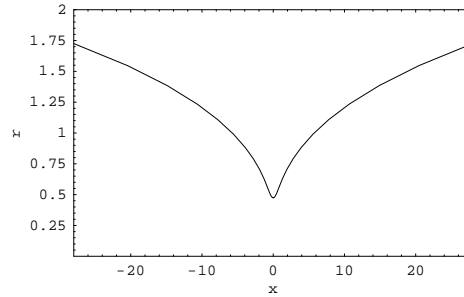
Figure 5: Jet profiles with no inertia for various power law exponents.

We next show symmetric jet profiles with inertia. We first consider the branch shown in Figure 4. Figure 6 shows three jet profiles along this branch, one near the middle, one near the bottom and one near the top. We note that there are two points on the branch with $a = 0.3$. The lower part of the branch is where the solution should be close to the inertialess case. Indeed the profile in Part a of Figure 6 or 7 is very similar to that in Part a of Figure 5 except for the scaling of ξ . This discrepancy in scaling naturally arises from the different nondimensionalizations which lead to the inertialess and, respectively, inertial solutions. As we approach the end of the branch, the jet profile collapses into $x = 0$.

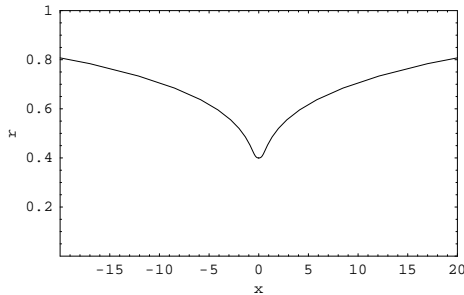
The magnification in Figure 7 illustrates the quadratic behavior near the origin at the lower end of the branch, while on the other hand, the profile becomes very flat at the upper end, where s_0 is close to σ_4 . This would be expected, since we get fourth order behavior in the limit.



(a) $a = 0.3$, lower branch

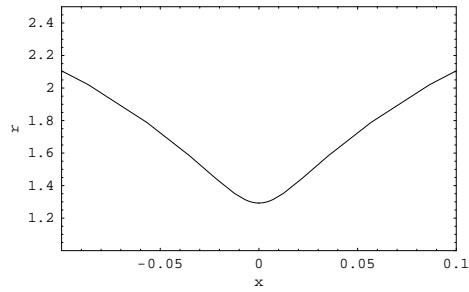


(b) $a = 0.3$, upper branch

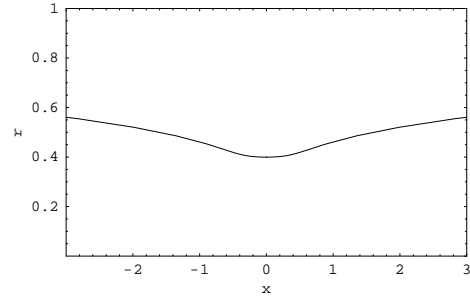


(c) $a = 0.18$

Figure 6: Jet profiles on symmetric branch for small power law exponent a .



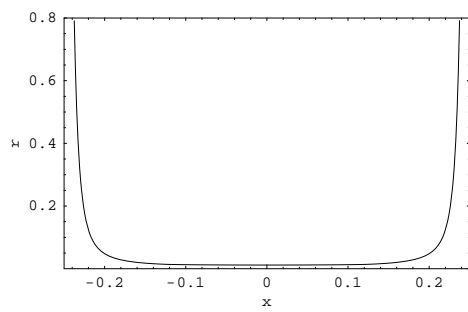
(a) $a = 0.3$, lower branch



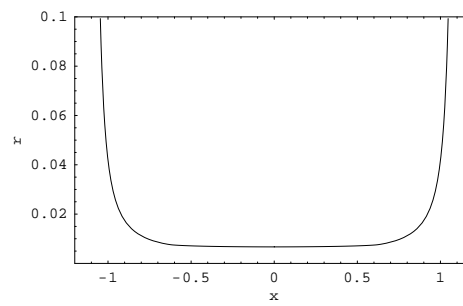
(b) $a = 0.18$

Figure 7: Symmetric branch for small a , refined views

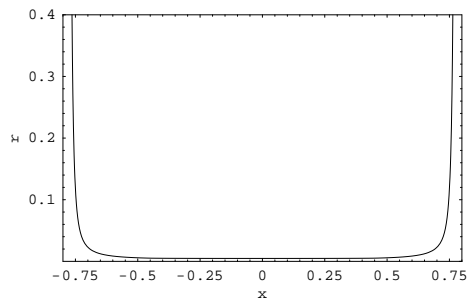
Figure 8 shows three jet profiles on the branch of symmetric solutions shown in Figure 3. The most obvious difference between the profiles is the shrinking of the horizontal coordinate as the endpoints of the branch are approached. If we were actually able to compute all the way to the endpoint, a singular limit would be approached in which the profile shrinks all the way to a point. If we blow up the ξ -variable, however, the profile coincides in this limit with the inertialess profile discussed before.



(a) $a = 1.954$



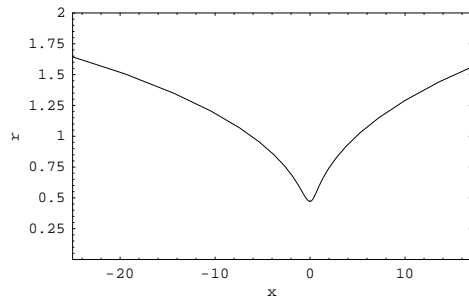
(b) $a = 1.9768$



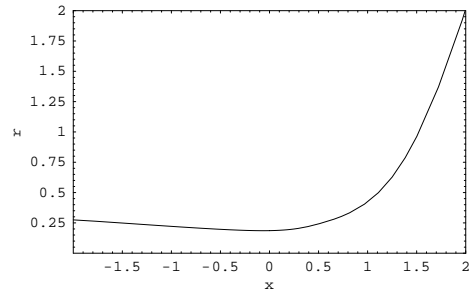
(c) $a = 1.9855$

Figure 8: Jet profiles on symmetric branch for large power law exponent a .

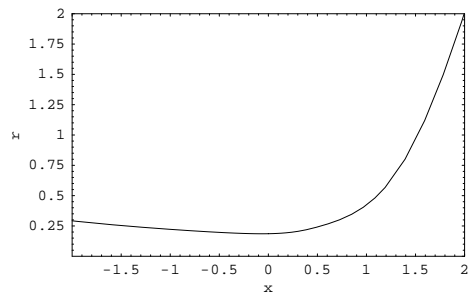
Figure 9 shows jet profiles on the Eggers branch. We note that the profile at $a = 0.31$ is close to that on the symmetric branch. In contrast, we found that the profiles at $a = 1.94$ and $a = 1.96$ are virtually identical to that at $a = 1.9$ and distinctly asymmetric. Near $a = 1$, the jet profile becomes extremely asymmetric, as is well known from the Newtonian case. The profiles become less asymmetric for either large or small values of a , and the Newtonian profile is actually the one that “looks” most asymmetric. We have not tried to quantify the degree of asymmetry; one possible measure is the value of u_0 , i.e. the velocity at the origin. This value, however, has its maximum near $a = 0.6$. We note that the discrepancy between β and the inertialess value of $\beta = 3a/2 + 1$ reaches its maximum near $a = 1$.



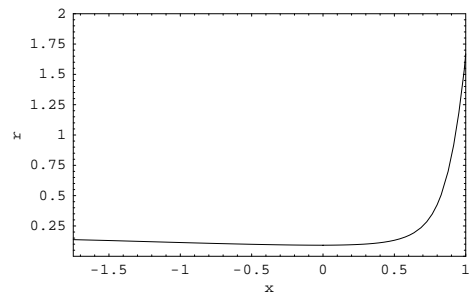
(a) $a = 0.31$



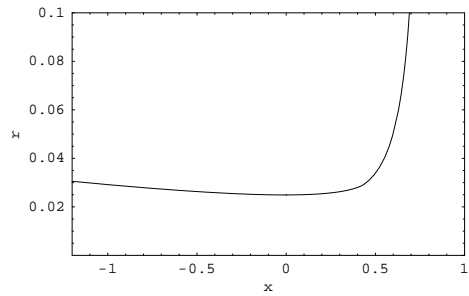
(b) $a = 0.5$



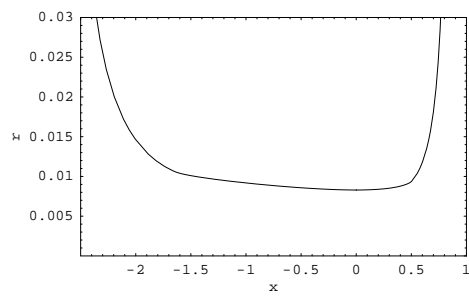
(c) $a = 0.7$



(d) $a = 1.0$



(e) $a = 1.5$



(f) $a = 1.9$

Figure 9: Jet profiles on the Eggers branch for various values of the power law exponent

6 Conclusions

We have investigated the existence of self-similar solutions for breakup of a jet of a power law liquid. Both flow with and without inertia was investigated. A branch of solutions continuing the Newtonian solution found by Eggers was found to exist for values of the power law exponent a between approximately 0.3 and 1.97. For small and large values of a , on the other hand, the assumption of neglecting inertia becomes self-consistent, and the inertialess solution, which exists for every positive a , is a valid solution even when inertia is present. Symmetric solutions with inertia were found for a near 0.3 and 1.97; these symmetric branches play a crucial role in the transition from inertialess to inertial behavior.

Acknowledgement

This research has been supported by the National Science Foundation under Grants DMS-0103813 and CTS-0090381.

References

- [1] A. Bach et al., Elongational viscosity of narrow molar mass distribution polystyrene, *Macromolecules* **36** (2003), 5174-5179.
- [2] M.P. Brenner, J.R. Lister and H.A. Stone, Pinching threads, singularities and the number 0.0304..., *Phys. Fluids* **8** (1996), 2827-2836.
- [3] P. Doshi et al., Scaling in pinch-off of generalized Newtonian fluids, *J. Non-Newton. Fluid Mech.* **113** (2003), 1-27.
- [4] P. Doshi and O.A. Basaran, Self-similar pinch-off of power law fluids, submitted to *Phys. Fluids*
- [5] V.M. Entov and E.J. Hinch, Effect of a spectrum of relaxation times on the capillary thinning of a filament of elastic liquid, *J. Non-Newton. Fluid Mech.* **72** (1997), 31-53.
- [6] J. Eggers, Universal pinching of 3d axisymmetric free surface flows, *Phys. Rev. Lett.* **71** (1993), 3458-3460.

- [7] J. Eggers, Nonlinear dynamics and breakup of free-surface flows, *Rev. Mod. Phys.* **69** (1997), 865-929.
- [8] J.R. Lister and H.A. Stone, Capillary breakup of a viscous thread surrounded by another viscous fluid, *Phys. Fluids* **10** (1998), 2758-2764.
- [9] D.T. Papageorgiou, On the breakup of viscous liquid threads, *Phys. Fluids* **7** (1995), 1529-1544.
- [10] M. Renardy, Self-similar jet breakup for a generalized PTT model, *J. Non-Newt. Fluid Mech.* **103** (2002), 261-269.
- [11] M. Renardy, Similarity solutions for jet breakup for various models of viscoelastic fluids, *J. Non-Newt. Fluid Mech.* **104** (2002), 65-74.
- [12] M. Renardy and D. Losh, Similarity solutions for jet breakup in a Giesekus fluid with inertia, *J. Non-Newt. Fluid Mech.* **106** (2002), 17-27.
- [13] A. Rothert, R. Richter and I. Rehberg, Transition from symmetric to asymmetric scaling function before drop pinch-off, *Phys. Rev. Lett.* **87** (2001), 4501-4504.